JOURNAL OF SOLID STATE CHEMISTRY 3, 26–38 (1971)

Conceptual Phase Diagram and Its Application to the Spontaneous Magnetism of Several Pyrites*

JOHN B. GOODENOUGH

Lincoln Laboratory, Massachusetts Institute of Technology, Lexington, Massachusetts 02173

Received August 1, 1970

A one-electron energy diagram is constructed for FeS_2, and its modification for CoS_2 and NiS_2 are discussed. A T–n_l–b phase diagram is constructed, where n_l gives the occupancy of the narrow σ^* band determined by chemistry and $b \sim \epsilon\lambda_\sigma$ is proportional to the width of the narrow σ^* band in the itinerant-electron domain. Here ϵ is a one-electron energy and λ_σ is the e_g-(sp^3) covalent-mixing parameter for σ-bonding orbitals. These two diagrams are used to interpret the varied magnetic properties of the systems $Fe_{1-x}Co_xS_2$, $Co_{1-x}Ni_xS_2$, $CoS_{2-x}Se_x$, and $CoS_{2-x}As_x$. In the mixed systems, the σ^* bands must be separated into donor and acceptor bands, and it is shown how this may be done for each system. The ferromagnetic to antiferromagnetic transition in $CoS_{2-x}Se_x$ is attributed to the appearance of a spin-density wave in the narrow transitional range of b between full-moment ferromagnetism ($\mu_{Co} = 1\ \mu_B$) and Pauli paramagnetism.

I. Energy Bands for Transition-Metal Pyrites

The pyrites, which have the formal chemical formula $M^{2+}(X_2)^{2-}$, contain interpenetrating face-centered cubic (fcc) cation and anion arrays, as in the rocksalt structure. However, the molecular $(X_2)^{2-}$ anions are not spherical, but have axial symmetry. Each of the four simple-cubic subarrays of the fcc $(X_2)^{2-}$ array have their molecular axes ordered along a different $\langle 111 \rangle$ direction, which gives an overall cubic symmetry to the crystal. As illustrated in Fig. 1, each cation is in the center of an anion octahedron, and each anion has a tetrahedral coordination consisting of one anion and three cations.

Construction of a one-electron energy diagram proceeds as follows: The energies of the isolated M^{2+} and $(X_2)^{2-}$ ions shown to the left in Fig. 2 are interchanged in a crystal because of the electrostatic Madelung energy, which can be readily calculated for a point-charge model. In any real crystal, charge transfer from the anions to the cations reduces the effective ionic charges, and hence the energy-level splitting $E_M - E_I$. In addition, the ionic interactions broaden the one-electron energy levels for the isolated ions into one-electron energy bands, as illustrated in Fig. 3. In this figure the left and right columns indicate the ionic one-electron levels, which are displaced relative to each other by the energy $E_M - E_I$. The transition-metal $3d$ orbitals are split by the cubic component of the crystalline fields into orbitals of e_g and t_{2g} symmetry. (A small trigonal component to the field splits the t_{2g} level.) The molecular-anion orbitals are represented by (sp^3) hybrids, one of which is split into occupied, anion–anion-bonding σ_A orbitals and unoccupied, anion–anion antibonding σ_A^* orbitals characteristic of σ-bonding orbitals in any X_2 molecule. The remaining three hybrid orbitals per anion σ bond covalently with the ($e_g^2 sp^3$) cation orbitals. This covalent interaction stabilizes the primarily anionic orbitals, broadening their energies into cation–anion-bonding σ bands; it destabilizes the primarily cationic orbitals, broadening their energies into cation–anion-antibonding σ^* bands. This is illustrated in the center column of Fig. 3. The narrow σ^* band of e_g symmetry at the center of the Brillouin zone Γ is not split by the translational symmetry of the fcc cation array. The band gap between the broad σ and σ^* bands should be as great as, or larger than, that found in ZnS, i.e., $E_g \approx 3.5$–4.0 eV, since Zn is the more acidic ion. Since the anion sp^3 orbitals are all active in strong σ bonding and the neighboring cations are at a relatively large distance, there is little covalent mixing with the cation t_{2g} orbitals to either destabilize them or transform them into

* This work was sponsored by the Department of the Air Force.

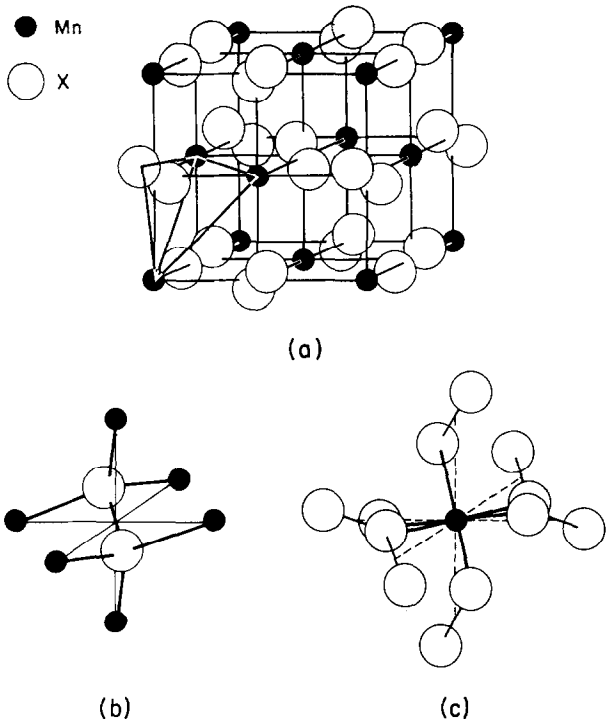

FIG. 1. The pyrite structure and near-neighbor coordinations of the cations and the anions.

itinerant electrons. Therefore they may be considered localized, and the splitting between the t_{2g} levels and the center of the σ^* band derived from e_g orbitals is large: $10Dq \gtrsim 2$ eV. This indicates that in the absence of intra-atomic exchange splitting, which is not shown in Fig. 3, the energy gap between the t_{2g} levels and the bottom of the lowest σ^* band, whose width we designate W_b, is $(10Dq - \frac{1}{2}W_b) \sim 1$ eV.

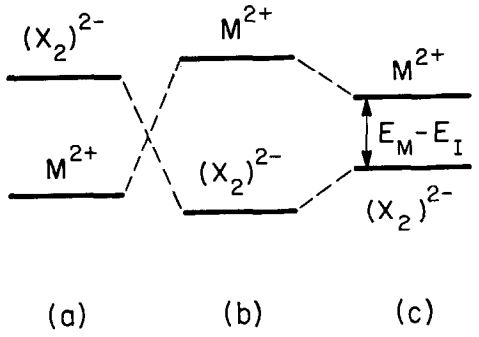

FIG. 2. Multielectron, ionic energy levels for purely ionic model of a pyrite M^{2+} $(X_2)^{2-}$: (a) isolated ions, (b) point-charge crystal, and (c) ionic crystal modified by ion polarization.

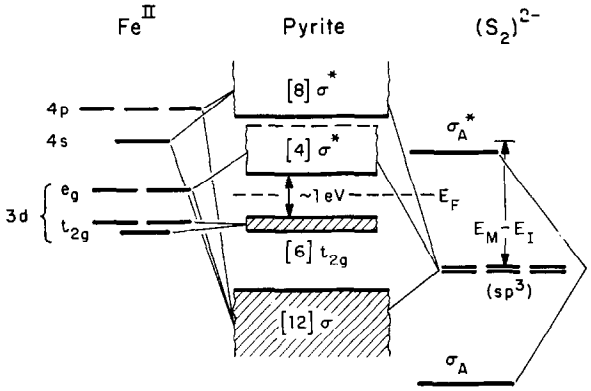

FIG. 3. One-electron energy levels for outer electrons of FeS_2 with the pyrite structure.

Splitting of the σ_A and σ_A^* orbitals may be estimated as about twice the stabilization energy of a single S–S bond. Pauling (*1*) gives a value of about 2.21 eV, which would place the σ_A^* level ~ 1 eV below the bottom of the broad σ^* bands.

The position of the *d* energies relative to the top of the occupied σ bands is more difficult to determine. However, for a given anion, the relative stabilities of the *d* orbitals increase as the cations go from left to right across any long series of the periodic table. From comparisons of the physical properties of other sulfides (*2*), the narrow σ^* bands associated with Fe^{2+}, Co^{2+}, and Ni^{2+} e_g orbitals seem to lie above the top of the σ bands, whereas those associated with Zn^{2+} e_g orbitals appear to fall below. The Cu^{2+} σ^* bands apparently overlap the σ bands, and whether the top of the σ^* bands falls below or above the top of the σ bands may be structure-dependent. The pyrites CuS_2, CuSSe, $CuSe_2$, CuSeTe, and $CuTe_2$ are all superconductors at lowest temperatures (*3*). Although suggestive, this does not require the existence of σ-band holes, since the σ^* bands may be broad ($b > b_{cs}$ in Fig. 9). For the systems $Fe_{1-x}Co_xS_2$ and $Co_{1-y}Ni_yS_2$, the Fermi energy may be assumed to lie above the top of the σ bands. In the cases of $CoSe_2$ and CoSAs, this assumption is more doubtful, but it forms the basis of the present discussion.

From these considerations, which have neglected any electron correlations, the six outer *d* electrons per molecule of FeS_2 would place the Fermi energy for this compound between filled t_{2g} orbitals and an empty σ^* band. CoS_2 would have the narrow σ^* band one-quarter filled, and NiS_2 would have this band half-filled. In CuS_2, there is one hole per molecule either in the narrow σ^* band, or shared between this and the σ bands. From this model,

which is essentially that suggested by Bither et al. (*3*), we predict FeS_2 to be a narrow-gap ($10Dq - \frac{1}{2}W_b \sim$ 1 eV) semiconductor, CoS_2 and NiS_2 to be narrow-band metals. Although FeS_2 is indeed found to be a narrow-gap semiconductor, CoS_2 is a ferromagnetic metal and NiS_2 is an antiferromagnetic semiconductor (*3*). These observations show that electron correlations within the narrow σ^* band cannot be neglected and that the pyrites provide a particularly interesting opportunity to study experimentally narrow-band electron correlations. The purpose of this paper is to compare data available for several pyrite systems with a conceptual T–n_l–b phase diagram. The temperature T and the band occupancy number n_l may be determined experimentally, but the transfer energy b, which parametrizes the strength of the interactions between electrons at near-neighbor cations, is not directly measurable. However, it may be directly related to the covalent-mixing parameter, which varies in a qualitatively known way for different elements. Hence the "conceptual" character of the diagram.

II. Conceptual Phase Diagram

A. Motivation

Crystal-field theory and band theory are the two limiting descriptions of the atomic outer electrons—the electrons outside of closed shells—once the atoms have come together to form a crystal. Crystal-field theory rests on the assumption that the interactions between the outer electrons on neighboring atoms are so weak that the electrons remain *localized* at discrete atomic positions for a time long compared to the period of the optical-mode atomic vibrations. Band theory, on the other hand, rests on the assumption that the interactions between the outer electrons on neighboring atoms are so strong that each electron is *itinerant*, being shared equally by all the like atoms of a periodic array.

The outer s and p electrons, which are primarily responsible for the binding energy of a crystal and therefore interact strongly with the neighboring atoms, may almost always be described by band theory. They form the broad σ and σ^* bands of Fig. 3 as well as the molecular σ_A and $\sigma_A{}^*$ energies. Outer f electrons, which are tightly bound to their nuclei and are screened from near-neighbor atoms by $5s^2 5p^6$ or $6s^2 6p^6$ core electrons, may always be described by a localized-electron model. The outer d electrons, on the other hand, are intermediate in character, and in the construction of Fig. 3 it was assumed that the d electrons of t_{2g} symmetry are localized, those of e_g symmetry form a narrow σ^* band of itinerant-electrons states. Since the t_{2g} orbitals are completely filled in the systems to be discussed, the localized-electron and itinerant-electron descriptions are equivalent, so no assumption other than band filling is involved. The character of the σ^* bands is the principal concern of this paper.

In the pyrites MnX_2, the Mn^{2+} ions carry a high-spin, localized atomic moment approaching 5 μ_B. The pyrites CuX_2 are metallic, without spontaneous magnetism, and become superconducting at lowest temperatures. Itinerant-electron σ^* orbitals are clearly indicated. The FeX_2 compounds have empty σ^* bands (unless the σ band overlaps the bottom of the σ^* band in $FeTe_2$), which eliminates electron correlations. Therefore empty itinerant-electron σ^* bands are correct for Fig. 3. However, electron correlations may be important in CoX_2 and NiX_2, where the narrow σ^* bands are partially filled. In the sulfides, electron correlations play a role, and conventional band theory, which neglects them, gives an inadequate description of the σ^* bands.

The intermediate character of the d electrons forces us to ask, and at the same time permits us to investigate experimentally, the following fundamental question: Do we have one thermodynamic state for the outer electrons with two limiting theories and a gradual transition in properties as we go from the conditions where one theory is applicable to those where the other is applicable; or do we have at least two thermodynamic states for the electrons, one described by a localized-electron model and the other by an itinerant-electron model? In order to investigate this question experimentally, it is useful to have a conceptual phase diagram in terms of the outer electrons. Although the pyrite systems to be discussed subsequently in this paper do not span the range of interaction-parameters b from localized electrons to uncorrelated, itinerant electrons, they do appear to span the range from correlated to uncorrelated itinerant electrons. (The pyrites MnS_2, $MnSe_2$, and $MnTe_2$ containing high-spin Mn^{2+} ions are not discussed.)

B. The Interaction Parameter

In the crystal-field limit and without cation–cation interactions, the outer d electrons of e_g symmetry are described by

$$\psi_e = N_\sigma(f_e - \lambda_\sigma \phi_\sigma), \qquad \lambda_\sigma = \frac{b^{ca}}{(E_e - E_\sigma)}, \quad (1)$$

where ϕ_σ represents the σ-bonding anion–hybrid orbitals of e_g symmetry and energy E_σ, f_e are the two

accidentally degenerate ionic d orbitals of e_g symmetry with energy E_e, and

$$b^{ca} \equiv (\psi_e, \mathscr{H}^{ca}\phi_\sigma) \sim \epsilon^{ca}(\psi_e, \phi_\sigma) \tag{2}$$

is the transfer energy for the cation–anion interaction. The energy operator $\mathscr{H}^{ca}$ represents the perturbation of the potential for the anion electrons by the presence of the cation, ϵ^{ca} is a one-electron energy, and λ_σ is known as the covalent-mixing parameter. Interactions between these localized e_g electrons on neighboring cations is introduced through the spin-independent transfer energy

$$b_{ij} \equiv (\psi_{ei}, \mathscr{H}'\psi_{ej}) \sim \epsilon_{ij}(\psi_{ei}, \psi_{ej}), \tag{3}$$

where the energy operator $\mathscr{H}'$ represents the perturbation of the potential for the crystal-field e_g electrons at cation-site position $\mathbf{R}_j$ by the presence of a neighboring cation at $\mathbf{R}_i$, and ϵ_{ij} is a one-electron energy. Since the cations are so far apart in the pyrite structure that the overlap integrals (f_{ei}, f_{ej}) are negligible, the transfer energy for nearest-neighbor cation–cation interactions is

$$b \sim \epsilon\lambda_\sigma{}^2 \sim \frac{\epsilon(\epsilon^{ca})^2(\psi_e, \phi_\sigma)^2}{(E_e - E_\sigma)^2}. \tag{4}$$

This is the interaction parameter to be used in construction of the phase diagram.

In the crystal-field limit, the electrostatic energy required to transfer an electron from one cation to its neighbor is U, as illustrated schematically in Fig. 4(a). Therefore admixture of the electron-transfer excited state requires second-order perturbation theory, and

$$\Delta\epsilon \approx -\frac{t_{ij}^2}{U}, \tag{5}$$

where t_{ij} is the spin-dependent transfer energy. To abstract the spin-independent part of this integral, use is made of the following relationship between spin components α, β and α', β' of $\mathbf{S}_i$ and $\mathbf{S}_j$ making an angle θ with one another:

$$\begin{aligned} \alpha &= \cos(\theta/2)\,\alpha' + \sin(\theta/2)\,\beta', \\ \beta &= -\sin(\theta/2)\,\alpha' + \cos(\theta/2)\,\beta'. \end{aligned} \tag{6}$$

Where there is one electron per e_g orbital ($n_l = 1$), the Pauli exclusion principle only allows transfer if the spins are antiparallel, so Eq. (5) becomes

$$\Delta\epsilon \approx -\left(\frac{b_{ij}^2}{U}\right)\cdot\sin^2(\theta/2) = \text{const} + \left(\frac{2b_{ij}^2}{4S^2U}\right)\mathbf{S}_i\cdot\mathbf{S}_j. \tag{7}$$

This is the origin of the antiferromagnetic *superexchange* contribution to the interatomic exchange interaction between localized spins,

$$\begin{aligned} \mathscr{H}_{ex} &= -\sum_{ij} J_{ij}\,\mathbf{S}_i\cdot\mathbf{S}_j, \\ J_{ij} &= J_{ij}^d + J_{ij}^S \approx J_{ij}^S, \\ 4S^2 J_{ij}(n_l = 1) &\approx -2b_{ij}^2/U. \end{aligned} \tag{8}$$

If there is one e_g electron per cation ($n_l = \frac{1}{2}$), then electrons transfer preferentially to the empty e_g orbital (the e_g orbitals are twofold-degenerate) and may have either spin with respect to the receiving cation. However, if the transferred-electron spin is parallel to the spin of the electron already present on the ion, then it is stabilized by the intra-atomic-exchange energy Δ_{ex} and

$$4S^2 J_{ij}^S(n_l = \tfrac{1}{2}) \approx -2b_{ij}^2\Delta(1/U) = +2b_{ij}^2\Delta_{ex}/U^2, \tag{9}$$

which is ferromagnetic. Similarly

$$4S^2 J_{ij}^S(n_l = \tfrac{3}{2}) = +2b_{ij}^2\Delta_{ex}/U^2. \tag{10}$$

These relations provide rules for the signs of the superexchange interactions as well as a guide as to how the magnitudes of these interactions vary with increasing transfer energy b_{ij}.

If there are a nonintegral number of electrons per like cation, ($n_l = 1 \pm c$, where $c \neq \frac{1}{2}$), electron transfer does not create an excited state, see Fig. 4(b), and first-order perturbation theory must be used. This gives the *double-exchange* stabilization

$$\Delta\epsilon_D = -ct_{ij} = -cb_{ij}^D\cos(\theta/2), \tag{11}$$

where from Eq. (6) the $\cos(\theta/2)$ angular dependence is taken because a mobile electron transfers without a change of spin from a full to a half-filled orbital, or from a half-filled to an empty orbital. This interaction is also ferromagnetic.

In the uncorrelated-band regime, electron transfer does not create an excited state for any n_l, and there

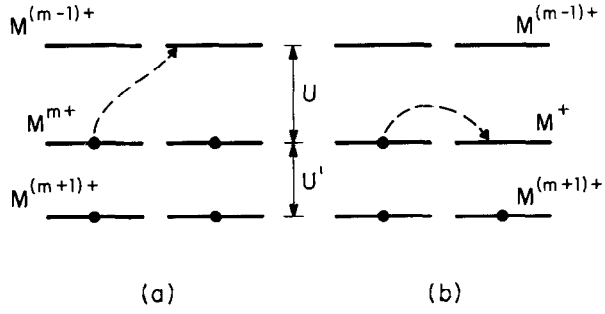

FIG. 4. Electron-transfer excited states entering (a) superexchange and (b) double exchange.

is no localized spin on the receiving cation. In tight-binding theory, this leads to a bandwidth

$$W_b \sim b. \tag{12}$$

C. Phase Diagram for $n_l = 1$

In the pyrite structure the nearest-neighbor interactions go through a single anion atom whereas the next-nearest-neighbor interactions go through both atoms of a molecular anion, as can be seen from Fig. 1. This suggests that the next-nearest-neighbor interactions are weaker than the nearest-neighbor interactions. However, both interactions are important, and any complete phase diagram must consider at least two transfer energies: b_{nn} and b_{nnn}. For simplicity, it is assumed that

$$b_{nn} = b \text{ and } b_{nnn} = \gamma b,$$

where $0 < \gamma \lesssim 1$ is a constant for all values of b. Although the magnitude of γ determines the type of magnetic order to be encountered where $J_{nnn} < 0$, the constraint $\gamma \neq \gamma(b)$ does not alter the qualitative physical arguments to be made.

Given this constraint and an $n_l = 1$, the antiferromagnetic Néel temperature for localized-electron magnetic ordering is proportional to $|J_{nn}|$, and from Eq. (8)

$$T_N \sim |J_{nn}| \approx |J^S_{nn}| \sim b^2/U. \tag{13}$$

Calculation of the energy U remains a central problem. In the localized-electron limit, $U \approx 15$ eV; in the uncorrelated-band limit a $U \approx 0$ is assumed. Mott (*4*) has argued that

$$U = (|\psi_e(1)|^2, V|\psi_e(2)|^2) \tag{14}$$

contains a screening parameter $\xi = \xi(b)$ in the electron–electron coulomb energy

$$V = (e^2/r_{12})\exp(-\xi r_{12}), \tag{15}$$

where $\xi(b)$ increases with b, but is otherwise unspecified. This gives a U that decreases continuously with increasing b; and U may change rapidly, if not discontinuously, with b in the transition region from localized to itinerant-electron behavior. It follows that in the range of b for which the superexchange perturbation expansion of Eq. (5) converges, T_N must increase with b as shown schematically in Fig. 5. This is the region of b for which a localized-electron theory is applicable.

In the broad-band limit, an $n_l = 1$ corresponds to a half-filled band having bandwidth W_b, as illustrated in Fig. 6. In this limit there is no spontaneous atomic moment, the crystal is metallic rather than insulating, and the magnetic susceptibility is weak

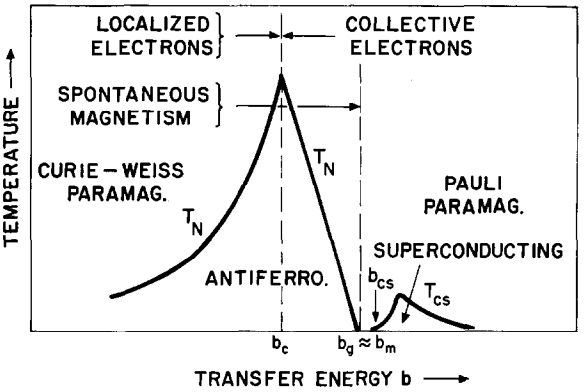

FIG. 5. Schematic T–b phase diagram for $n_l = 1$.

and temperature-independent. (Pauli paramagnetism: $\chi_m = 2\mu_B{}^2 N(\epsilon_F)$.) In this limit, a transition from a normal conductor to a superconductor may be anticipated below a T_{cs}, the magnitude of T_{cs} increasing with $N(\epsilon_F)$ as b decreases.

In the intermediate range, the two energy levels M^{m+} and $M^{(m-1)+}$ must broaden and decrease their energy separation with increasing b (see Fig. 6) until the bands overlap at some critical value $b = b_g$. Here one band is formed, but a deep minimum may remain in the density-of-states $N(E)$ versus energy E curve for a small range of $b > b_g$. This would be reflected in an exchange enhancement of the magnetic susceptibility and a quenching of the superconducting transition temperature T_{cs}. Furthermore, in the interval $b_c < b < b_g$, electron correlations induce an energy gap that is not allowed by the translational symmetry of the crystal (*5*). However, antiferromagnetic order can enhance this splitting by creating a new translational symmetry that introduces a Brillouin-zone boundary near the

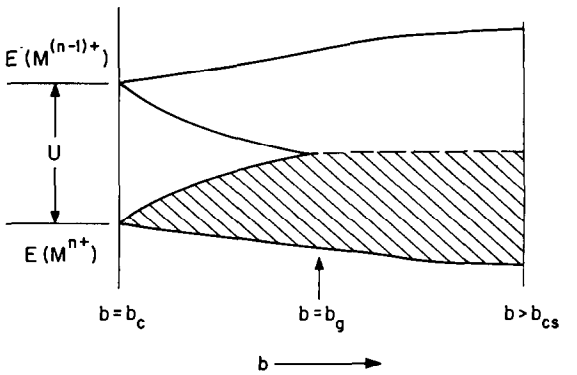

FIG. 6. Variation of pseudoparticle energy levels with increasing b for the case $n_l = 1$.

Fermi energy. Therefore itinerant-electron antiferromagnetism should occur in this range, T_N increasing with decreasing b. Whether this T_N joins smoothly the localized-electron T_N, as shown in Fig. 5, depends upon whether there is a first-order transition on going from the localized-electron regime ($b < b_c$) to the itinerant-electron regime ($b > b_c$). Furthermore, whether T_N decreases smoothly to zero at a $b_m \approx b_g$ depends upon whether there is a first-order transition on going from correlated to uncorrelated itinerant electrons. From previous work on isostructural series of oxides, it has been possible to infer (*6*) that the transitional region $b_c < b < b_g$ is narrow, which explains why itinerant-electron magnetism is a relatively rare phenomenon. This makes particularly important studies of the transition-metal pyrites, which exhibit itinerant electron magnetism in narrow bands that are not overlapped by broad s or p bands.

D. Phase Diagrams for $n_l = 1 \pm c$

If there are a nonintegral number of electrons/atom present in a band, corresponding to $n_l = 1 \pm c$, then in the limit $b < b_m$ the concentration, c, of mobile charge carriers adds to the antiferromagnetic superexchange coupling $J\mathbf{S}_i \cdot \mathbf{S}_j$, the ferromagnetic double-exchange coupling of Eq. (11). Minimization of this sum with respect to the angle θ between $\boldsymbol{S}_i$ and $\boldsymbol{S}_j$ gives an equilibrium cant angle θ_0 defined by

$$\cos(\theta_0/2) = c/c_f; \quad c_f = 4|J|\,S^2/b^D. \tag{16}$$

Thus as c increases, there may be a continuous change from antiferromagnetism at $c = 0$ to ferromagnetism for $c > c_f$, as indicated in the n_l–b diagram for $T = 0°K$ shown in Fig. 7. In the itinerant-electron region $b_c < b < b_g$, the existence of a Fermi surface would stabilize an antiferromagnetic spiral (AFS) spin configuration with turn angle θ_0 in the absence of an external magnetic field H_a, but the field H_a may induce an AFS to ferromagnetic, canted (C) transformation. This is known as *metamagnetism*.

Definition of b_c is probably less sharp where there are a nonintegral number of electrons per cation, but it is still a meaningful concept (*7*). If the time for an electron to transfer from one cation to its neighbor is long compared to an optical-mode vibration period of the crystal, then the electrons become trapped at localized atomic positions by nuclear displacements. Such an entity, electron or hole plus local crystal distortions, is called a *small polaron*, and small polarons are distinguished from bare electrons by the line $b = b_c$. Polaron–polaron

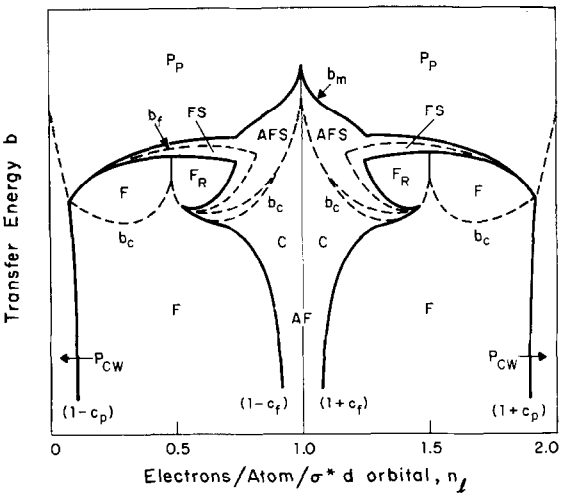

FIG. 7. Schematic n_l–b diagram for $T = 0°K$. The critical parameters are: b_c = localized versus itinerant electron bonding, b_f = boundary defined by $U_{\text{eff}}N(0) > 1$, F = ferromagnetic domain, F_R = ferromagnetic domain with reduced moment $\mu_R = 2c\mu_B$, P_p = Pauli paramagnetic domain, P_{cw} = Curie–Weiss paramagnetic domain, C = canted-spin ferromagnetic domain, AFS = antiferromagnetic-spiral domain, FS = ferromagnetic-spiral domain, AF = antiferromagnetic order along the line $n_l = 1$.

interactions must suppress b_c from its value where there are nearly an integral number of electrons per cation. In the case of the doubly degenerate σ^* bands in the transition-metal pyrites, integral numbers of electrons per cation occur at $c = 0, \frac{1}{2}, 1, \frac{3}{2}$, and 2.

The criterion for spontaneous band ferromagnetism is given by

$$U_{\text{eff}}N(0) > 1, \tag{17}$$

where $N(0)$ is the density of states at the Fermi surface at $T = 0°K$ and U_{eff} is the effective value of the electrostatic energy U (*8*, *9*). This gives $b = b_f$ in Fig. 7. For smaller values of c and a Fermi surface ($b > b_c$) to make an AFS spin configuration more stable than a canted-spin configuration, the criterion for spontaneous magnetism replaces $N(0)$ in Eq. (17) by the function

$$F(Q) = \frac{2\Omega}{(2\pi)^3} \int_{\epsilon_{\mathbf{K}} < \epsilon_F} \frac{d^3k}{(\epsilon_{\mathbf{K}+\mathbf{Q}} - \epsilon_{\mathbf{k}})}, \tag{18}$$

which reflects perturbations of the one-electron energies by the wavevector $\mathbf{Q}$ of the AFS configuration (*10*).

At $c = \frac{1}{2}$, there is one electron per cation in a twofold-degenerate σ^* band, and the dominant correlations are ferromagnetic, corresponding to

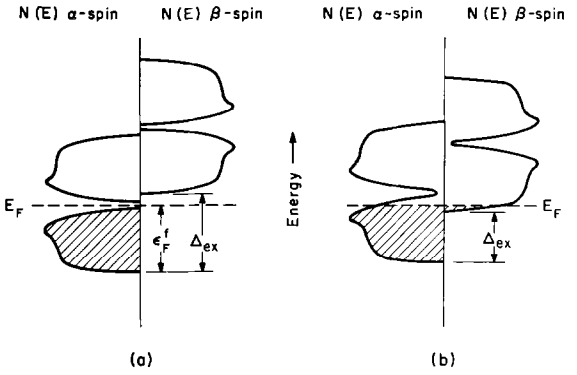

FIG. 8. Exchange splitting Δ_{ex} of states of α and β spin for $c = \frac{1}{2}$: (a) $\Delta_{ex} > \epsilon_F{}^f$ and (b) $0 < \Delta_{ex} < \epsilon_F{}^f$.

Eq. (9). In the range $b_c < b < b_f$, the states of α and β spin are shifted relative to one another, as shown in Fig. 8. The electron correlations simultaneously split the α-spin and β-spin energies in two because there are an integral number of electrons per cation. For small enough b, we should expect to find a ferromagnetic semiconductor. For larger b, both the exchange splitting Δ_{ex} and any isospin-band gap are reduced; and where $0 < \Delta_{ex} < \frac{1}{2}W_b$ the compound is metallic with a reduced magnetic moment. The down-spin electrons create spin-density waves below the magnetic ordering temperature, and interactions with the Fermi surface would introduce standing spin-density waves of large amplitude (*11*). Whether this gives rise to ferromagnetic-spiral (FS) or antiferromagnetic-spiral (AFS) spin configurations depends upon the magnitude of the exchange splitting Δ_{ex}, and it is logical to anticipate a change from a FS to an AFS configuration as $b \to b_m$, where $\Delta_{ex} \to 0$. This idea is illustrated schematically in Fig. 9, the T–b diagram for $n_l = \frac{1}{2}$. A similar change would occur for localized electrons coupled via mobile electrons as the mobile-electron bandwidth increases from $b \approx b_c$, where double exchange is applicable, to larger b where a Rudermann–Kittel–Yosida–Kasuya theory must be used.

In general, the overlap of occupied α-spin and β-spin states occurs if $\Delta_{ex} < \epsilon_F{}^f$, where $\epsilon_F{}^f$ is the energy difference between the Fermi surface and the bottom of the α-spin band when only α-spin states are occupied. Clearly, a larger c (smaller n_l) reduces the possibility of having a FS to AFS transition with increasing b, a smaller c (larger n_l) enhances it. In fact, AFS configurations may occur over two different ranges of b if $\frac{1}{2} < n_l < 1$ (or $\frac{1}{2} > c > 0$), provided electron correlations split the α-spin and β-spin bands in two. The first transition separates a ferromagnetic domain F having the maximum possible atomic moment

$$\mu = 2(1 - c)\,\mu_B, \tag{19}$$

to a reduced moment in which only bonding states are occupied,

$$\mu_R = 2c\,\mu_B. \tag{20}$$

The second transition separates the domain of reduced ferromagnetic moment F_R from the paramagnetic domain P_p. This is schematically illustrated by Fig. 10, the T–b diagram for $n_l = \frac{2}{3}$, and is also indicated in Fig. 7.

III. The System $Fe_{1-x}Co_xS_2$

The compound FeS_2 is a semiconductor (optical band gap of 0.9 ± 0.1 eV) without spontaneous magnetism (*3*), as might be anticipated from Fig. 3. CoS_2 is metallic and ferromagnetic: $T_c = 122°K$, $\mu_{Co} = 0.84$–$0.88\ \mu_B$, and from measurements of

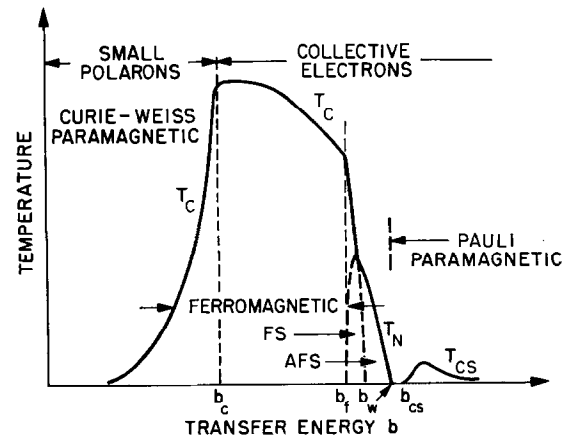

FIG. 9. T–b diagram for $n_l = \frac{1}{2}, \frac{2}{3}$.

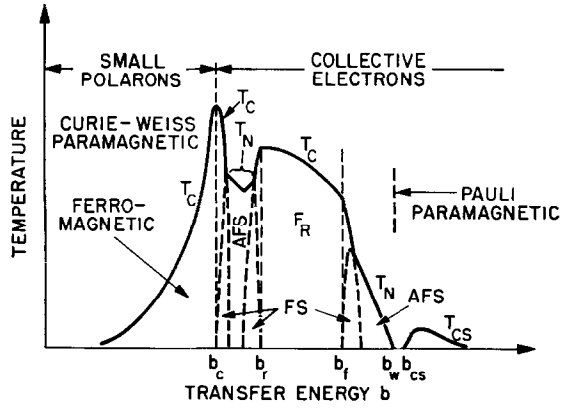

FIG. 10. T–b diagram for $n_l = \frac{2}{3}, \frac{4}{5}$.

magnetic susceptibility χ_m below 500°K, $\mu_{eff}^2 \approx 4.5$ μ_B^2, $\theta_p = 150$°K (*12*). Although other workers (*13–15*) have reported a break in the slope of χ_m^{-1} versus T that is associated with changes in the thermal expansion coefficient and the temperature dependence of the resistivity, Mikkelson and Wold (*12*) find that diamagnetic corrections to the measured susceptibilities eliminate this anomaly. Furthermore, the other changes at 400°K are not clearly defined, if present at all. Measurements of χ_m to higher temperatures (*13–15*) may give values for μ_{eff}^2 that more nearly approach the theoretical value of 3 μ_B^2 for a localized spin $S = \frac{1}{2}$, but always $\mu_{eff}^2 > 3.0\ \mu_B^2$. On the other hand, the magnetization at $T = 0$°K is clearly smaller than the theoretical value of 1 μ_B/Co atom for completely spin-polarized σ^* electrons.

These data immediately suggest itinerant-electron ferromagnetism in the limit of small intraband exchange splitting: $0 < \Delta_{ex} < \epsilon_F{}^f$, as illustrated in Fig. 8(b). Furthermore, in this limit the slope of the χ_m^{-1} versus T plot ($C_m^{-1} \approx 8\ \mu_B{}^2/\mu_{eff}^2$) tends to be too small, which makes μ_{eff}^2 too large, as shown in Fig. 11(a). As pointed out by Jarrett et al. (*15*), this inference appears to be confirmed by the system $Fe_{1-x}Co_xS_2$, which exhibits ferromagnetism with a magnetization at $T = 0$°K of $\mu_0 = x\ \mu_B$ per molecule over the range $0.05 < x < 0.95$, but a moment that decreases with increasing x in the range $0.95 < x < 1.0$.

Superficially, the system $Fe_{1-x}Co_xS_2$ corresponds to $n_l = x/2$. With this model, the magnetic data are consistent with Fig. 7, an $x \approx 0.05$ corresponding to $c_p \approx 0.975$ and the bandwidth $W_b \sim b$ increasing sufficiently that the system passes from the F to the FS region of the diagram at $x \approx 0.95$. This interpretation, though suggestive, is superficial because a rigid-band model is totally inadequate. The inadequacy was demonstrated (*15*) by the observation that Ni substitutions $Co_{0.75-2y}Ni_yFe_{0.25+y}S_2$, which keep the total number of d electrons constant, give a decrease in μ_0 comparable to an antiparallel coupling of nearly 2 μ_B per Ni^{2+} ion in the range $y < 0.1$.

A more realistic model must recognize that the energy of a heavier Co(II) ion is lower than that of an Fe(II) ion. From data on thiospinels, a high-spin Co^{2+} ion has its d-state manifold about 0.6 eV below that of a high-spin Fe^{2+} ion (*2*), and approximately the same energy difference can be anticipated for the low-spin cations. Therefore the Co(II) ions substitute into FeS_2 as relatively deep donor ions, and at lower temperatures the electrons of the σ^* band are all trapped at the Co(II) ions. This modifies the energy-level diagram of Fig. 3 in the following way: For $x \ll 0.05$, isolated Co(II) ions form donor e_g levels below the σ^* band that trap the x added electrons per molecule at lowest temperatures. Interactions between these trapped electrons are weak, so there is no spontaneous magnetism. This situation corresponds to $c > c_p$ in Fig. 7. For $x > 0.05$, the Co(II) ions form an impurity Co(II)-ion σ^* band below the Fe(II)-ion σ^* band. For smaller x, this band is so narrow that $\Delta_{ex} > \epsilon_F{}^f$,

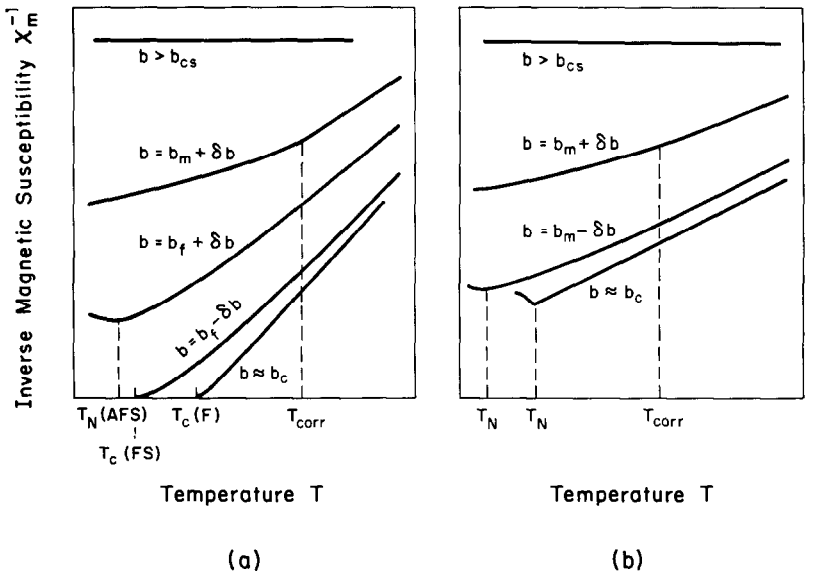

FIG. 11. Inverse susceptibility versus temperature for various values of $b = b_m \pm \Delta b$: (a) $n_l = \frac{1}{2}$, (b) $n_l = 1$.

corresponding to Fig. 8(a), and it has a ferromagnetic moment $\mu_s = x\ \mu_B$. However, from Fig. 8(a) we should anticipate semiconducting rather than metallic behavior, unless there is either some overlap of the impurity cobalt band and the host iron band or there is only a minimum, instead of a gap, in the density-of-states versus energy curve at the Fermi energy.

According to Fig. 9, the strength of the Co–Co interactions is relatively insensitive to the bandwidth W_b where $\Delta_{ex} > \epsilon_F{}^f$, so T_c and θ_p increase with the number of Co–Co interactions per molecule, and hence with x. However, W_b for the Co(II)-ion σ^* band increases whereas W_b for the Fe(II)-ion σ^* band decreases with increasing x; and from the FS configuration of CoS_2, corresponding to Fig. 8(b), it is necessary to anticipate a F to FS transition in the Co(II)-ion σ^* band with increasing x. The data of Jarrett et al. (*15*) indicate that this transition occurs at an $x_c < 0.95$. According to Fig. 9, the strength of the Co–Co interactions decreases more rapidly with increasing x as $x \to x_c$, and especially for $x > x_c$. Therefore, although the number of Co–Co interactions continues to increase with x, the sum of their strengths, which is proportional to $T_c \approx \theta_p$, may actually decrease with increasing x as $x \to x_c$, and the model provides a convenient, though qualitative, interpretation for the observed maximum in $T_c \approx \theta_p$ at $x \approx 0.75 < x_c$.

Similarly, a Ni^{2+} ion would be a donor to the Co(II)-ion σ^* band and a deep donor to the Fe(II)-ion σ^* band. Therefore two electrons are trapped in the two localized e_g orbitals at an isolated Ni^{2+} ion, and intra-atomic exchange stabilizes the triplet ($S = 1$) state. The observation (*15*) that isolated Ni^{2+}-ion spins are coupled antiparallel to the spin of the ferromagnetic Co(II)-ion σ^* band requires either that the dominant superexchange electron transfer is from the σ^* band to the half-filled e_g orbitals of a Ni^{2+} ion or, which seems more reasonable, that the dominant transfer of e_g electrons is to the β-spin σ^* band. This latter condition is assured provided the splitting of bonding and antibonding α-spin states, which is indicated in Fig. 8(a), is large enough to raise the antibonding α-spin energies above the bottom of the β-spin bands. This proposition is reasonable, especially at $x \approx 0.75$ where x approaches x_c.

IV. The System $Co_{1-x}Ni_xS_2$

The σ^* band of NiS_2 is half filled ($n_l = 1$), and any spontaneous magnetism would exhibit antiferromagnetic order. However, according to Eqs. (12) and (4) the σ^* bandwidth $W_b \sim b$ should increase with decreasing $(E_e - E_g)$, and hence on going to the right in the periodic table from Fe(II) to Co(II) to Ni^{2+}. Although this change may be offset somewhat by the possibilities for an intra-atomic exchange stabilization between the two outer electrons per Ni^{2+} ion, experience indicates that the former effect dominates, so we should entertain the possibility that NiS_2 may exhibit no spontaneous magnetism. This is not found. Stoichiometric NiS_2 appears to be antiferromagnetic with a complex magnetic order and an atomic moment $\mu_{Ni} = 1.17\ \mu_B$ (*16*). Nevertheless other samples of NiS_2 (presumably slightly nonstoichiometric) appear to have no spontaneous atomic moment (*13*, *17*). Furthermore, a Néel temperature $T_N \approx 40°K$, a $\mu_{Ni} = 1.17\ \mu_B$, a $\mu_{eff} > 3.1\ \mu_B$ and a very large, negative $\theta_p < 1500°K$ (*3*, *18*) make clear that NiS_2 only just fulfills the criterion for spontaneous band magnetism. Furuseth et al. (*17*), who found no spontaneous antiferromagnetism in their NiS_2, observed a change of slope in χ_m^{-1} versus T at $440 \pm 40°K$, electrical-resistivity and thermal-expansion anomalies also occurring at this temperature. This may reflect a change from weakly correlated to strongly correlated electron states in the σ^* band, μ_{eff} changing from $3.15\ \mu_B$ for $T < 440°K$ to $2.7\ \mu_B$ for $T > 440°K$.

For example, if we ask how the χ_m^{-1} versus T plot should change as b increases from $b \approx b_c$ to $b > b_m$, we might anticipate the series of curves illustrated in Fig. 11(b). For smaller b, a localized-electron model gives a good description, the reciprocal slope of the line giving a $C_m = 1$, corresponding to a $\mu_{eff} \approx 2.83\ \mu_B$, and the intercept θ_p having a magnitude $|\theta_p| < 5T_N$. At larger $b > b_{cs}$ a weak, temperature-independent Pauli paramagnetism gives a large, temperature-independent ($\theta_p \to -\infty$) reciprocal susceptibility. A continuous variation from one limit to the other would be characterized by a series of χ_m^{-1} versus T plots each appearing to obey a Curie–Weiss law within any limited temperature range, but giving a μ_{eff} and a $|\theta_p|$ that are too large at lower temperatures for any meaningful interpretation in terms of atomic moments and interatomic exchange interactions. In the magnetically ordered state, on the other hand, spin transfer from one sublattice to the other reduces the atomic moment μ_A. This accounts well for the marked discrepancy between the $\mu_{Ni} = 1.17\ \mu_B < 2\ \mu_B$ obtained from neutron-diffraction measurements in the ordered state and the paramagnetic susceptibilities, which give a $\mu_{eff} > 2.83\ \mu_B$ (except as extrapolated from highest temperatures) with a $|\theta_p| \sim 400T_N$.

Significantly, antiferromagnetic NiS_2 is semiconducting (*3*, *16*), which suggests that where the electron correlations are strong enough to induce spontaneous magnetism, they are strong enough to open up an energy gap in the middle of the σ^* band, i.e., $b_m \approx b_g$. With only one atom per primitive unit cell in the fcc cation array, the σ^* band would not be split in two above T_N by the translational symmetry of the lattice. However, the different orientations of the $(X_2)^{2-}$ molecules makes the primitive cell cubic, and translational symmetry may contribute to the splitting.

In the system $Co_{1-x}Ni_xS_2$, initial substitutions of Ni^{2+} ions couple antiferromagnetically to the Co(II)-ion σ^* band, indicating that two σ^* electrons are trapped at each Ni^{2+}-ion donor center. For larger values of x, no clear evidence of spontaneous magnetic order has been reported, except for the end member $x = 1.0$. This finding suggests that where the Ni^{2+}-ion σ^* impurity band is formed, all long-range order of the correlations is destroyed. Long-range order only just reappears as $x \to 1.0$ ($n_l \to 1$), where the crystal becomes a semiconductor.

V. The System $CoS_{2-x}Se_x$

The isoelectronic substitution of Se for S leaves the σ^* bands one-quarter filled ($n_l = \frac{1}{2}$, $c = \frac{1}{2}$) and perturbs the primarily cationic, narrow σ^* band less than does a cation substitution for the Co(II) ion. In general, the heavier Se^{2-} ion can be expected to bond covalently more strongly than the S^{2-} ion, thereby giving a larger λ_σ and hence a greater bandwidth $W_b \sim b \sim \epsilon\lambda_\sigma$. If this reasoning is valid, then $NiSe_2$ should have a broader σ^* band than NiS_2 and hence have a half-filled, uncorrelated σ^* band. Indeed $NiSe_2$ is metallic (no correlation or symmetry splitting) and has only a weak, Pauli paramagnetism (*17*). Therefore, if CoS_2 has a FS spin configuration, then from Fig. 9 the broader σ^* band of $CoSe_2$ can be expected to support either an AFS spin configuration or no spontaneous magnetism. Neutron-diffraction experiments on $CoSe_2$ provide conflicting findings: Adachi et al. (*13*) find antiferromagnetic order below about 93°K, whereas Furuseth et al. (*17*), found no magnetic order down to 4°K in their sample. These findings suggest that stoichiometric $CoSe_2$, like stoichiometric NiS_2, just sustains spontaneous magnetic order, which is quite consistent with the appearance of an AFS configuration in a narrow range of b between a FS configuration and the paramagnetic state P, as illustrated in Fig. 9. It is therefore intriguing that T_N should be so high in the sample exhibiting magnetic order. It is nearly as high as the Curie temperature $T_c \approx 122$°K found in CoS_2, and it suggests that T_N may drop abruptly on passing from correlated to uncorrelated itinerant-electron states. In this connection, it is perhaps significant that the $CoSe_2$ sample without spontaneous antiferromagnetic order shows a change in slope of the χ_m^{-1} versus T plot with an associated anomaly in the thermal expansion similar to that found in NiS_2, μ_{eff} changing from 2.30 to 2.05 μ_B (*17*). This would be consistent with a higher order transition from a weakly correlated to a strongly correlated σ^* band at a temperature T_{corr}. If $T_N > T_{corr}$, magnetic order would stabilize the strongly correlated state to lowest temperatures. However, if $T_N < T_{corr}$, it may drop abruptly with increasing b.

An alternative view of $CoSe_2$ is to assume that the top of the σ bands overlaps the Fermi energy in the selenium compounds, thus increasing n_l in the σ^* bands. This possibility seems less attractive, but it cannot be eliminated definitively without further experimentation. However, the σ bands certainly do not overlap the Fermi energy in $FeSe_2$, which is a semiconductor like FeS_2 (*3*). The fact that $\mu_{eff} > 1.73$ μ_B in $CoSe_2$ need not indicate the presence of more than one σ^* electron per Co^{II} ion, since the slopes (C_m^{-1}) of the χ_m^{-1} versus T plots should vary as illustrated in Fig. 11(a) on passing from $b \approx b_c$ to $b > b_m$.

Johnson and Wold (*19*) found that in the system $CoS_{2-x}Se_x$, the ferromagnetic, atomic moment in a field of 10 kOe at 4.2°K remains nearly constant throughout the range $0 \leqslant x \leqslant 0.20$, but decreases abruptly in the range $0.20 < x \leqslant 0.25$. The Curie temperature decreases linearly to about 55°K at $x = 0.2$, but abruptly in the range $0.20 < x \leqslant 0.25$. A minimum in χ_m^{-1} versus T near 90°K for all $x \geqslant 0.20$ suggests the presence of antiferromagnetic order below this temperature and a ferromagnetic to antiferromagnetic transition at $T_c < T_N$ in the range $0.20 \leqslant x \leqslant 0.25$. There is little variation in μ_{eff} across the system (*13*, *19*), which is consistent with the top of the σ band remaining below the Fermi energy.

Substitution of a heavier Se^{2-} ion for an S^{2-} ion would tend to lift σ^* states from below the Fermi energy to above it, because of the larger covalency of the heavier anion. (The σ^* bands are antibonding with respect to cation–anion interactions.) Since Se additions lift states from the bottom of the bonding band, they tend to remove an equal number of α-spin and β-spin states from below the Fermi energy to above it, leaving μ_0 nearly constant. Therefore it need not be surprising that the observed $\mu_0 = 0.88$ μ_B

per cobalt atom remains nearly constant throughout the range $0 \leqslant x \leqslant 0.20$. On the other hand, the Curie temperature T_c and the Weiss constant θ_p each reflect the summation of all the near-neighbor ferromagnetic interactions; and for initial substitutions of Se, the Co–S:Se–Co interactions are eliminated because the larger covalency of selenium anions lifts associated σ^* states above the Fermi energy. This accounts nicely for the decrease in T_c and θ_p with increasing x. For $x \geqslant 0.20$, negative interactions enter to make $\theta_p < T_c$, θ_p eventually becoming negative for $x > 0.6$. Presumably these are not individual Co–S:Se–Co interactions, but itinerant-electron interactions within a Co–S:Se–Co σ^* band that overlaps the Fermi energy more and more with increasing $x \geqslant 0.20$.

VI. The System $CoS_{2-x}As_x$, $0 < x < 1$

Substitution of arsenic for sulfur is similar to substitution of selenium, except that $n_l = (1 - x)/2$ instead of remaining constant. If the arsenic p orbitals remain below the Fermi energy, then stoichiometric CoSAs should be a semiconductor with a weak, temperature-independent diamagnetic susceptibility, its Fermi energy falling between filled t_{2g} orbitals and an empty σ^* band at the low-spin Co(III) ions. Mikkelson and Wold (*12*) report a small, temperature-dependent paramagnetism with a $\theta_p \approx 0$, which they suggest may be due to deviation from stoichiometry. This interpretation is probably correct. The anion distribution is not ordered, and small sulfur-rich regions would be ferromagnetic, but sufficiently isolated from other such regions that no long-range magnetic order occurs. Furthermore, $(As_2)^{4-}$ ions do not seem to form, so that sulfur-rich regions would be compensated by a small loss of arsenic, probably resulting in finely dispersed CoAs + As. Therefore there is no compelling reason not to accept the simplest model for stoichiometric, homogeneous CoSAs, viz., a Fermi energy between filled t_{2g} orbitals and empty σ^* bands.

The presence of two different anions complicates the σ^* bands. Itinerant-electron orbitals associated with Co–S:As–Co interactions are less stable than those associated with Co–S:S–Co interactions, since arsenic is the more covalent anion. It is precisely this complexity that permits capture of any σ^* electrons in the sulfur-rich regions of the crystal.

As in the selenium-substituted system, initial substitutions of arsenic lift σ^* states from below the Fermi energy to above it. Unlike the selenium-substituted system, there is a simultaneous reduction in the occupancy of the σ^* band, so that consistency with the nearly constant magnetic moment per cobalt ion in the range $0 < x < 0.20$ in $CoS_{2-x}Se_x$ would seem to require an initial *increase* in the magnetization per σ^* electron in the $CoS_{2-x}As_x$ system. Significantly, Mikkelson and Wold (*12*) found such an increase, the magnetization per σ^* electron reaching a maximum value of 1 μ_B at $x \approx 0.15$.

Again by analogy with the selenium-substituted system, the Curie temperature T_c and Weiss constant θ_p should decrease as the number of Co–S:S–Co interactions is reduced, the Co–S:As–Co interactions being eliminated at those concentrations where the Co–S:As–Co acceptor σ^* band lies above the Fermi energy. In $CoS_{2-x}Se_x$ the acceptor orbitals seem to lie above E_F over the range $0 < x \leqslant 0.15$, if not all the way to $x = 0.20$. Since $n_l = (1 - x)/2$ in $CoS_{2-x}As_x$, this condition should hold to at least as large an x, or over the interval $0 \leqslant x \leqslant 0.15$. This reasoning suggests that T_c and θ_p should decrease with x at about the same rate in both $CoS_{2-x}Se_x$ and $CoS_{2-x}As_x$ over the range $0 \leqslant x \leqslant 0.15$, as has been observed by Mikkelson and Wold (*12*), and that this coincidence is not accidental.

For $x > 0.2$, on the other hand, a $\theta_p < T_c$ develops in the system $CoS_{2-x}Se_x$, whereas $\theta_p \approx T_c$ for all x in the system $CoS_{2-x}As_x$. If a $\theta_p < T_c$ reflects negative magnetic interactions via occupied states of a Co–S:Se–Co σ^* band, which overlaps the Fermi energy more and more with $x > 0.2$ in $CoS_{2-x}Se_x$, then a $\theta_p \approx T_c$ in $CoS_{2-x}As_x$ requires either that the Co–S:As–Co σ^* band remains above the Fermi energy for all x, or that it is too broad to sustain spontaneous ferromagnetism. Since the arsenic anion has a formal valence As^{3-}, the Co–S:As–Co σ^* band should be too broad for spontaneous magnetism. Furthermore, the maximum in μ_0 per σ^* electron at $x \approx 0.15$ is logically attributed to overlapping of the Fermi energy by the Co–S:As–Co σ^* band for $x > 0.15$, as illustrated in Fig. 12. If this σ^* band does not sustain spontaneous magnetism, it contributes nothing to θ_p and introduces β-spin electrons that reduce the magnetization per σ^* electron. However, this σ^* band does not eliminate different α-spin and β-spin populations so long as the bottom of the ferromagnetic Co–S:S–Co σ^* band falls below that of the Co–S:As–Co σ^* band, as shown in Fig. 12. Therefore $\theta_p \approx T_c$ and μ_0 decrease monotonically with the occupancy of the Co–S:S–Co σ^* orbitals, going to zero as $x \to 1.0$. However, deviations from homogeneity permit trapping of some σ^* electrons in isolated, sulfur-rich regions within nominal CoSAs.

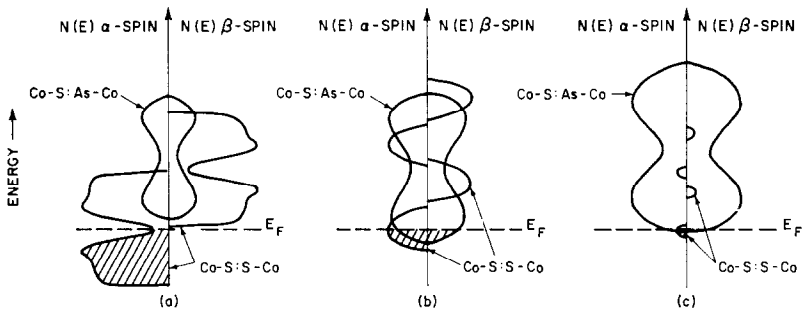

FIG. 12. Acceptor Co–S:As–Co and donor Co–S:S–Co σ^* bands in $CoS_{2-x}As_x$: (a) $x = 0.15$, (b) $x = 0.6$, (c) $CoS_{1+\delta}As_{1-\delta}$.

The slope (C_m^{-1}) of the χ_m^{-1} versus T curve is determined primarily by the occupancy of the Co–S:S–Co σ^* band. At high temperatures, where thermal narrowing tends to lift the bottom of the Co–S:As–Co σ^* band above the Fermi energy, this occupancy would decrease linearly with x. Mikkelson and Wold (*12*) found a $\mu_{eff}^2 = 4.5(1 - x)\ \mu_B{}^2$ in the range $0 < x < 0.5$, and only small deviations (to lower values) from this in the range $0.5 < x < 1.0$.

VII. Conclusions

This study, though based on physical reasoning rather than quantitative calculations, has shown the following:

(1) Useful one-electron energy diagrams can be constructed from simple symmetry arguments and a knowledge of the periodic table.

(2) A generalized phase diagram can be constructed that harmonizes well our knowledge of spontaneous magnetism, provided rigid-band models are judiciously modified in the case of mixed systems.

(3) The interesting magnetic properties of the pyrite mixed systems containing CoS_2 as one end member can be interpreted without the introduction of any ad hoc assumptions.

(4) The ferromagnetic to antiferromagnetic transition in the system $CoS_{2-x}Se_x$ appears to reflect overlapping of the Fermi energy by a Co–S:Se–Co σ^* band that supports AFS spin configurations, and this change from FS to AFS magnetic order on going to the broader σ^* band seems to be characteristic of the transition from F to FS to AFS to P as b increases through the interval $b_f - \Delta b < b < b_f + \Delta b$ in the neighborhood of $n_l = \frac{1}{2}$.

(5) The Co–S:As–Co σ^* band has $b > b_m$.

(6) The μ_{eff} obtained from the slope (C_m^{-1}) of χ_m^{-1} versus T is larger than or equal to that predicted for spin-only, localized-electron magnetism so long as electron correlations are active; but there is a sharp, probably continuous change with increasing b to temperature-independent, Pauli paramagnetism on passing to the uncorrelated domain. However, a discontinouus change may occur at a T_{corr}.

(7) The Weiss constant θ_p goes to $-\infty$ within a narrow range Δb as b increases from $b < b_m$ to $b > b_m$.

(8) Where electron correlations within a half-filled band are strong enough to induce spontaneous antiferromagnetism, they may be strong enough to split the band in two.

(9) Narrow bandwidths should decrease with increasing temperature, and higher-order transitions above room temperature in NiS_2 and $CoSe_2$ may reflect changes from weak to strong electron correlations.

(10) The superconductivity of CuX_2 pyrites may be due to either an overlap of the Fermi energy by the broad σ bands or a $b > b_{cs}$ for the narrow σ^* bands. More experiments are needed to distinguish between these alternatives.

References

1. L. PAULING, "The Nature of the Chemical Bond," 3rd ed., p. 85, Cornell Univ. Press, Ithaca, N.Y. 1960.
2. J. B. GOODENOUGH, *J. Phys. Chem. Solids* **30**, 261 (1969).
3. T. A. BITHER, R. J. BOUCHARD, W. H. CLOUD, P. C. DONOHUE, AND W. J. SIEMONS, *Inorg. Chem.* **7**, 2208 (1968).
4. N. F. MOTT, *Proc. Phys. Soc. London Sect. A* **62**, 416 (1949).
5. J. HUBBARD, *Proc. Roy. Soc. London Ser. A* **276**, 238 (1963).

6. J. B. GOODENOUGH, *J. Appl. Phys.* **39**, 403 (1968).
7. J. B. GOODENOUGH, *Mater. Res. Bull.* **5**, 621 (1970).
8. J. HUBBARD, *Proc. Roy. Soc. London Ser. A* **277**, 237 (1964).
9. J. KANAMORI, *Progr. Theor. Phys.* **30**, 275 (1963).
10. P. LEDERER AND A. BLANDIN, *Phil. Mag.* **14**, 363 (1966).
11. A. W. OVERHAUSSER, *Phys. Rev.* **128**, 1437 (1962).
12. J. MIKKELSON AND A. WOLD, *J. Solid State Chem.* **3**, 39 (1971).
13. K. ADACHI, K. SATO, AND M. TAKEDO, *J. Appl. Phys.* **39**, 900 (1968); *J. Phys. Soc. Jap.* **26**, 631 (1969).
14. S. MIYAHARA AND T. TERANISHI, *J. Appl. Phys.* **39**, 896 (1968).
15. H. S. JARRETT, W. H. CLOUD, R. J. BOUCHARD, S. R. BUTLER, C. G. FREDERICK, AND J. L. GILLSON, *Phys. Rev. Lett.* **21**, 617 (1968).
16. J. M. HASTINGS AND L. M. CORLISS, *IBM J. Res. Develop.* **14**, 227 (1970).
17. S. FURUSETH, A. KJEKSHUS, AND A. F. ANDRESEN, *Acta Chem. Scand.* **23**, 2325 (1969).
18. R. BENOIT, *J. Chim. Phys.* **52**, 119 (1955).
19. V. JOHNSON AND A. WOLD, *J. Solid State Chem.*, **2**, 209 (1970).